Acoustic emission (AE) fatigue-crack source modeling and simulation using moment tensor concept

Joseph, Roshan, Giurgiutiu, Victor

Roshan Joseph, Victor Giurgiutiu, "Acoustic emission (AE) fatigue-crack source modeling and simulation using moment tensor concept," Proc. SPIE 11379, Sensors and Smart Structures Technologies for Civil, Mechanical, and Aerospace Systems 2020, 113791J (26 May 2020); doi: 10.1117/12.2559958

SPIE.

Event: SPIE Smart Structures + Nondestructive Evaluation, 2020, Online Only, California, United States

Acoustic emission (AE) fatigue-crack source modeling and simulation using moment tensor concept

Roshan Joseph, Victor Giurgiutiu

Department of Mechanical Engineering, University of South Carolina, Columbia, USA

1 ABSTRACT

Acoustic emission (AE) is a well-developed structural health monitoring method that relies on capturing the elastic waves generated by the energy released during crack formation in a solid medium. Modeling and simulation of the AE due to various phenomena in the crack is essential to separate the AE due to different sources. A novel modeling approach based on moment tensor concept is presented in this paper to simulate AE due to fatigue crack. Fatigue cracking is a common problem in metallic structures during service life under cyclic loading conditions. The formation and growth of fatigue crack can cause catastrophic failure in metallic structures. AE signals are used to infer that cracks are growing in a structure during operation. However, it was found that fatigue crack may produce AE signals even without crack growth being present. These non-crack-growth AE signals in metallic structures can be caused by crack rubbing/clapping, which is a potential source of acoustic emission. The fatigue-crack growth-related AE needs to be separated from crack rubbing/clapping AE to understand the signals originating from the crack and to comprehend the situation of the crack in real-time. The AE source due to fatigue crack rubbing/clapping was assumed as a component of the moment tensor source, and the simulation was performed. An experiment was performed to record AE during a fatigue experiment. The fatigue AE signals were recorded using a 'MISTRAS micro-II digital AE system.' The simulation results were compared with experimental observations, and a good agreement of simulation and experiment was observed.

2 INTRODUCTION

For mechanical components that are frequently subjected to variable loading, fatigue cracking is a common problem. Acoustic emission technique was widely used for damage detection and source localization in metallic structures. The rubbing and clapping of fatigue crack faying surfaces can potentially cause an acoustic emission source. This paper aims at the study of fatigue crack acoustic emission signals due to crack growth and fatigue crack rubbing/clapping. The modeling of fatigue crack rubbing/clapping AE signals is also discussed in this paper.

AE signals may be generated by a wide range of phenomena such as micro-cracks, friction in existing cracks, dislocations, phase transformations, etc. The AE wavefield generated by an AE event propagates in thin-wall structures such as plates in the form of guided waves. Many researchers studied AE due to various kinds of sources. Acoustic emission in thin plates during crack growth event was investigated in many studies [1], [2]. Acoustic emission due to rubbing in a rotor-bearing and source localization was studied by Wang et al. [3]. Acoustic emission in composite materials was also studied for progressive damage in a polymer-based composite[4]; clustering of AE signals obtained from failure in carbon fiber reinforced plastic (CFRP) specimens was also studied [5]. Acoustic emission during various fracture activities was studied to relate the fracture and AE signals [2], [6]–[8]. McBride et al. [9] investigated the relationship between acoustic emission amplitude and the size of intermetallic inclusions at the fracture face. Barile et al. [10] used the acoustic emission technique to monitor delamination in a unidirectional CFRP

Sensors and Smart Structures Technologies for Civil, Mechanical, and Aerospace Systems 2020
edited by Haiying Huang, Hoon Sohn, Daniele Zonta, Proc. of SPIE Vol. 11379, 113791J
 · doi: 10.1117/12.2559958

subjected to mode I loading. They concluded that it is possible to follow delamination effects in CFRP through proper monitoring of variation of the AE features. Various studies on acoustic energy harvesting were reported in the literature [11]–[13].

Many researchers have done numerical and theoretical modeling and simulation of AE signals. Some of the studies performed numerical modeling of AE signals using Lamb waves[14], [15]. Finite element modeling and simulation of AE forward problem was performed [16]–[19]. Monopole or dipole definition of AE sources was used for modeling AE sources in several studies[20]. Definition of AE source by considering the AE source as a self-equilibrating seismic moment tensor was studied, and analytical formulations were developed for half-space and bulk medium in many pieces of research [21] [22]. In a recent study of AE guided wave propagation in a plate [23], the AE source was modeled as Helmholtz excitation potentials.

Even though AE due to various phenomena were reported, not many research works were conducted on AE due to rubbing and clapping of crack faying surfaces of thin sheet metals. It is a problem of practical interest since it is important to distinguish between AE due to crack rubbing and crack growth during fatigue crack growth events. This paper presents the detection of AE signals due to crack growth and crack rubbing/clapping in thin metallic sheet metal samples and the numerical modeling of AE signals due to fatigue crack rubbing/clapping.

The organization of this paper is as follows. First, this paper discusses the experimental methods used for the generation of AE signals due to rubbing and clapping of crack faying surfaces. In this section, the manufacturing of the cracked specimen and experimental set-up for the detection of fatigue crack AE signals are discussed. Then, the theoretical modeling of fatigue crack rubbing/clapping AE signals were discussed in detail. Next, the results of AE signals from fatigue crack during fatigue crack growth experiment and numerical prediction of fatigue crack rubbing/clapping AE signals are discussed. Finally, this paper ends with a summary, conclusions and future work.

3 EXPERIMENTAL METHODS

An AE experimental specimen was designed for capturing AE during crack growth in thin metallic plates. From a large plate of aluminum 2024-T3, coupons of 103 mm width, 305 mm length and 1 mm thickness were machined using the shear metal cutting machine. Specimens were sufficiently wide enough to allow a long crack to form in the specimen. A pre-crack of 4 mm tip to tip length was generated in the specimen through fatigue crack growth (Figure 1). After AE sensor instrumentation was installed on the specimen, the crack was grown an additional 5.4 mm (until the crack length reached 9.4 mm tip to tip), simultaneously capturing the AE signals. The wide geometry of the specimen was desired for this work so that the acoustic waves generated would travel a longer distance to the edges. This hypothesis, in turn, means the signals die out after reflection from the clay boundaries due to geometric spreading and material damping before reaching the sensors. The properties of Al 2024-T3 were modulus of elasticity 73 GPa, density 2767 kg/m3, and Poisson's ratio 0.33.

Two PWAS sensors and two S9225 sensors were bonded to the aluminum specimen. Clay boundaries were provided on the specimen to avoid reflection of AE signals from the specimen boundaries. PWAS sensors were bonded at a distance of 6 mm and 25 mm from the crack in a linear configuration. S9225 sensors were also bonded to the specimen at 6 mm and 25 mm from the crack in the opposite direction to the PWAS sensors. The specimen bonded with sensors is

presented in Figure 2. PWAS sensors were bonded using M-Bond AE-15 adhesive. This adhesive is appropriate for bonding PWAS because it is resilient to the dis-bonding of PWAS during long durations of cyclic loading. M-Bond AE-15 is an epoxy system with two components: a resin, and a curing agent. The resin and curing agent were mixed in a specific proportion and stirred for 5 minutes. PWAS was bonded to the specimen using the mixture and cured for 3 hours at 140^0F as recommended by the epoxy manufacturer. The capacitance of the PWAS was measured before bonding and after bonding to make sure that the PWAS, as well as the bonding of the PWAS to the specimen, was defect-free. The two S9225 sensors were bonded to the specimen using hot glue. A drop of hot glue was applied to the specimen using a hot gun, and the sensors were placed on the drop with the application of thumb pressure. The thumb pressure was continuously applied until the hot glue was cured.

Figure 1 Experimental set up for fatigue crack growth. Cyclic fatigue loading was applied to the specimen by mounting the specimen on the MTS machine.

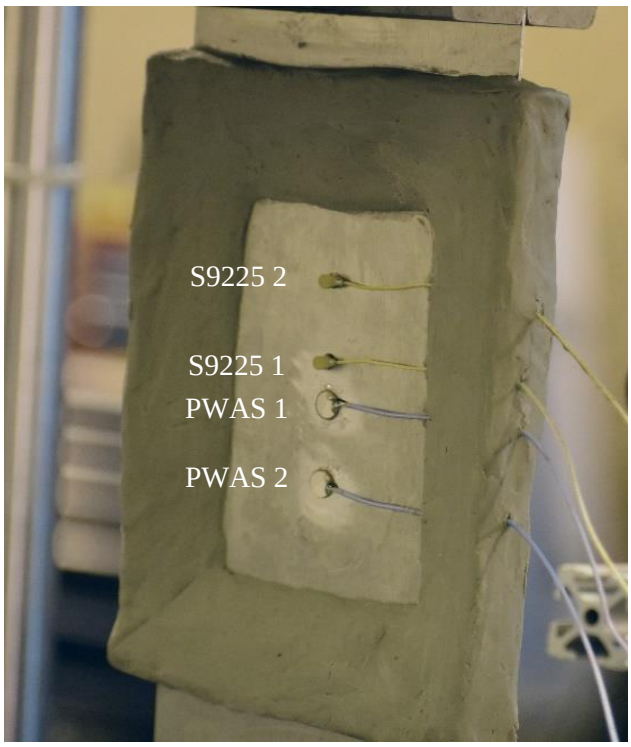

Figure 2 AE test specimen bonded with the two-PWAS and two-S9225 sensors. Non-reflective clay boundaries (NRB) were provided on the specimen to avoid the reflection of AE signals from the specimen boundaries.

After installing the sensors, the fatigue loading was continued to grow the crack and capture AE signals simultaneously. The test specimen installed with PWAS and S9225 transducers was mounted on the MTS machine (Figure 2). After the crack initiation and installation of sensors, the fatigue loading was continued to vary between 13.85 kN and 1.38 kN with a loading rate of 2 Hz with simultaneous capture of the AE signal. The experimental setup for capturing the AE signal from a fatigue crack growth event is presented in Figure 3. AE signals during crack growth events were captured by using PWAS and S9225 sensors. The sensors were connected to the acoustic preamplifier. The acoustic preamplifier is a bandpass filter, which can filter out signals between 30 kHz to 700 kHz. Provided with 20/40/60 dB gain (can be select using a switch), this preamplifier operates with either a single-ended or differential sensor. In the present experiment, 40 dB gain was selected. The preamplifier was connected to the MISTRAS AE system. A sampling frequency of 10 MHz was chosen to capture any high-frequency AE signals. The timing parameters set for the Mistras system were peak definition time (PDT)= 200μs, hit definition time (HDT)= 800 μs, and hit lockout time (HLT)= 1000 μs.

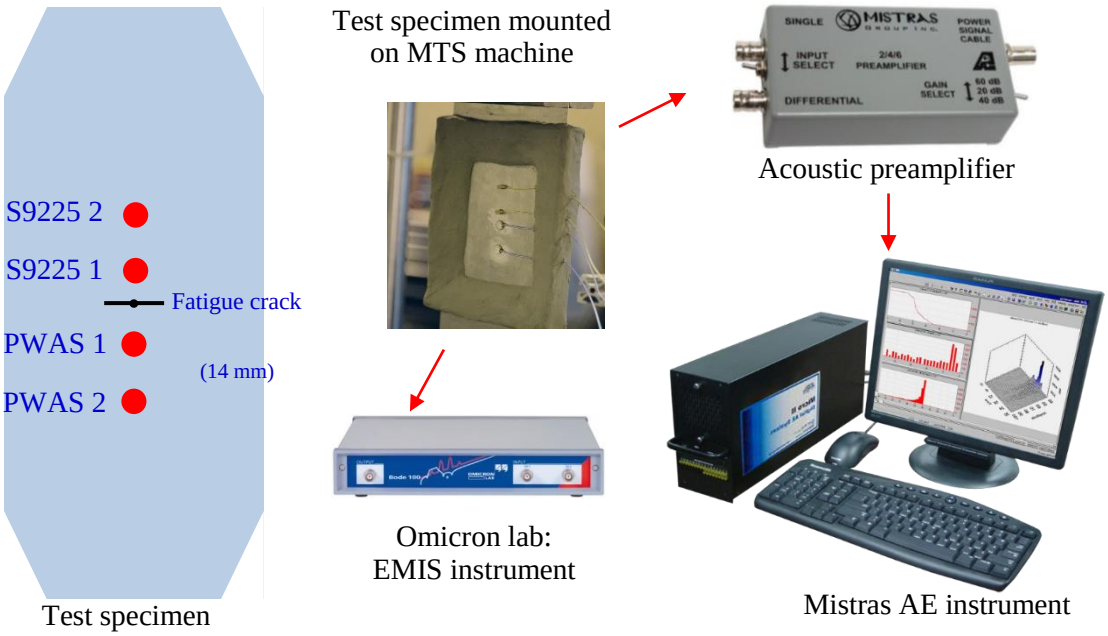

Figure 3 Experimental setup for capturing AE signals during fatigue crack event

4 THEORETICAL MODELING OF FATIGUE CRACK RUBBING/CLAPPING AE

The predictive modeling of fatigue crack rubbing/clapping was performed based on the physics of AE source excitation. The modeling methodology for fatigue crack rubbing/clapping is presented in Figure 4. When the crack faying surfaces come close to each other, the peaks and valleys of the surfaces rub/clap. Details of the rubbing/clapping of the peaks and valleys of the crack faying surfaces are shown in Figure 4c. When one pair of valley and peak rub each other, an equal and opposite force acts at the peak and valley. This couple force acts as the excitation source for producing the AE signal. The couple-forces are in the x-direction (or 1-direction), and the separation is in the y-direction (or 2-direction). So, the force couple can be considered as a moment M_{12} of the moment tensor. Therefore, the modeling of the AE source was performed by using M_{12} excitation source.

The schematic of the moment excitation acting on a 1D waveguide specimen is presented in Figure 5. A through-thickness M_{12} excitation was considered to produce Lamb wave propagation in a thin plate of thickness 2d. The thickness of the specimen, 2d, considered for the simulation, is 1 mm. At a distance of 25 mm from the AE-source location, a PWAS of 7 mm diameter was considered as a receiver.

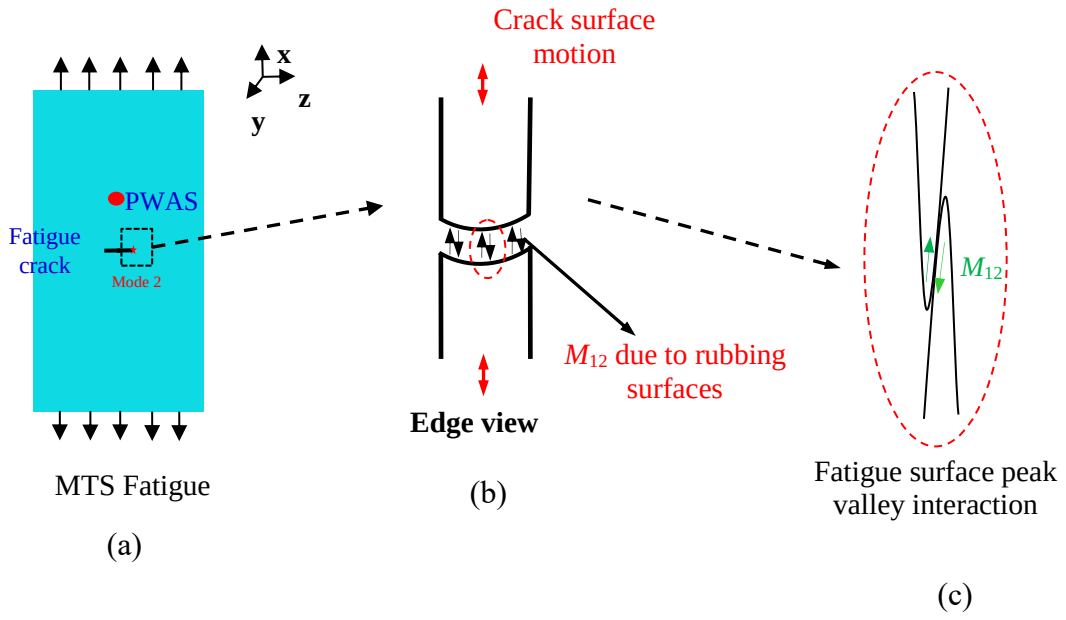

Figure 4 Fatigue crack rubbing/clapping AE signal source modeling methodology

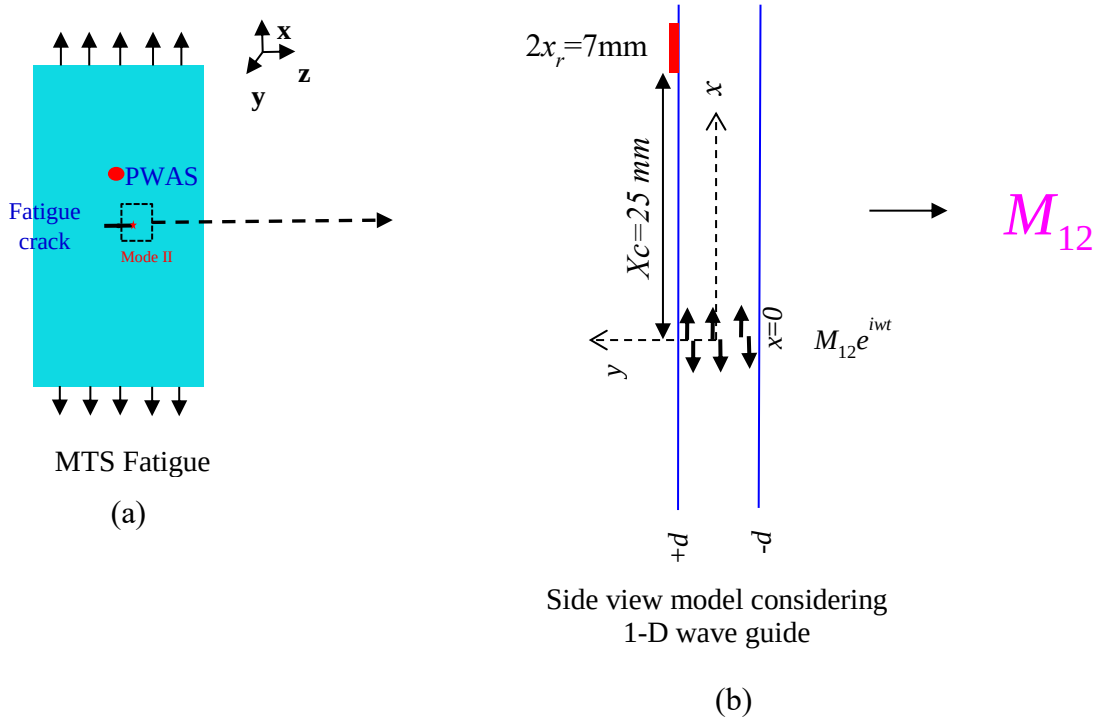

Figure 5 Fatigue crack rubbing/clapping AE source moment tensor representation

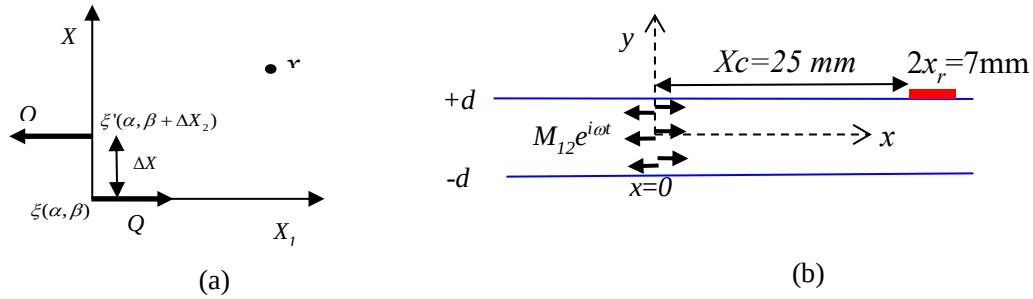

Figure 6 The through-thickness M_{12} moment excitation

Two force excitations separated by an infinitesimal distance creates a couple-moment excitation, as shown in Figure 6a. The limiting process of the separation turns the excitation to a moment excitation and the wavefield to the wavefield due to the moment. The through-thickness M_{12} moment excitation is presented in Figure 6b. The wavefield due to moment excitation can be obtained from the displacement field due to force excitation from the limiting process explained as following [22]

$$u_{Q_1}^{M_{12}}(x) = \lim_{\substack{\Delta X_2 \to 0 \\ Q_1 \to \infty \\ Q_1 \Delta X_2 \to M_{12}}} [Q_1 \Delta X_2] \left[\frac{G(x;\alpha,\beta) - G(x;\alpha,\beta+\Delta X_2)}{\Delta X_2}\right] = \frac{\partial G(x;\alpha,\beta)}{\partial X_2} \qquad (1)$$

Here, Q_1 is the monopole force excitation, and $G(x;\alpha,\beta)$ is the Green function of the excitation.

Following the limiting process in Eq.(1), from the velocity field due to in-plane force excitation in Ref. [24], the velocity field due to the M_{12} line source is obtained from the Eq. (1) as following

$$\text{Velocity, } v_{M_{12}} = \frac{\partial}{\partial y}(v_{F_x}) = \sum_m \frac{F_x}{4P_{mm}} \left[v_m(y)(\tilde{v}_x^m(y)_{-d}^{+d}) + v_m'(y) \int_{-d}^{d} \tilde{v}_x^m(y) dy \right] e^{-i\xi_m(x)} \qquad (2)$$

Here v_{F_x} is the velocity field due to an in-plane monopole force excitation F_x. The Lamb wave thickness mode shape is represented by $v_m(y)$. P_{mm} is the Lamb wave power flow. The wavenumber is represented by ξ_m.

The displacement field can be obtained from the velocity field as follows

$$\text{Displacement, } u_{M_{12}} = v_{M_{12}}/(i\omega) = \sum_m \frac{F_x}{4P_{mm}} \left[v_m(y)(\tilde{v}_x^m(y)_{-d}^{+d}) + v_m'(y) \int_{-d}^{d} \tilde{v}_x^m(y) dy \right] e^{-i\xi_m(x)} / i\omega \qquad (3)$$

The in-plane strain is the spatial derivative of the displacement field and can be obtained as follows

$$\text{Strain, } S_{M_{12}} = \frac{\partial}{\partial x}(u_{M_{12}}) = \sum_m -i\xi_m \frac{F_x}{4P_{mm}} \left[v_m(y)(\tilde{v}_x^m(y)_{-d}^{+d}) + \frac{\partial}{\partial y} v_m(y) \int_{-d}^{d} \tilde{v}_x^m(y) dy \right] e^{-i\xi_m(x)} / i\omega \qquad (4)$$

The strain field is sensed by the PWAS and converted to the equivalent voltage by the PWAS. The total voltage sensed by PWAS can be obtained from the integral as follows [24].

$$V_{M_{12}}^{PWAS} = \int_{S_c} V_3 = \frac{g_{31}^2}{(s_{11}^E \beta_{33}^T C_c)} \int_{S_c} \varepsilon_{xx} \mathrm{d}S \quad (5)$$

Here g_{31} is the piezoelectric voltage coefficient, s_{11}^E is the compliance of the PWAS, β_{33}^T is the impermittivity coefficient of the PWAS, C_c is the capacitance of the PWAS S_c is the surface area of the PWAS, ε_{xx} is the in-plane strain due to the AE.

Substituting Eq. (4) in Eq. (5) and simplifying, we get a closed-form expression for the voltage sensed by the PWAS as following

$$V_{M_{12}}^{PWAS} = \frac{g_{31}^2}{(s_{11}^E \beta_{33}^T C_c)} \sum_m \frac{F_x}{4P_{mm}} \left[v_m(y)(\tilde{v}_x^m(y)_{-d}^{+d}) + \frac{\partial}{\partial y} v_m(y) \int_{-d}^{d} \tilde{v}_x^m(y) dy \right] \times (e^{-i\xi_m(r_c+2s_r)} - e^{-i\xi_m(r_c)})/i\omega \quad (6)$$

The PWAS Lamb wave response due to M_{12} moment excitation is plotted using the expression in Eq. (6) and is presented in Figure 7. We observe a strong A0 mode response due to the excitation and no S0 wave mode generation was observed.

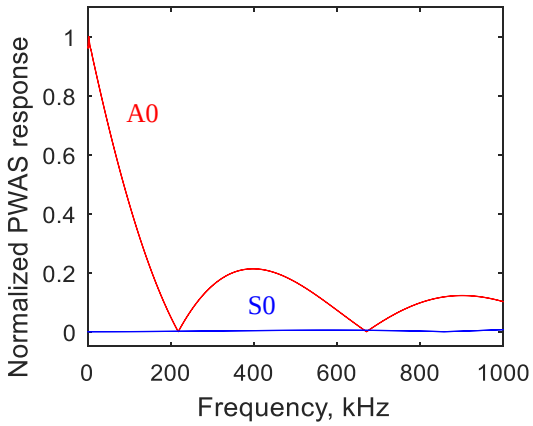

Figure 7 Lamb wave strain response due to M_{12} excitation on 1-mm thick aluminum specimen received with 7 mm PWAS receiver

5 RESULTS AND DISCUSSION

Fatigue experiment was performed to record the AE during a fatigue crack growth event. Based on the frequency spectrum of the AE signals observed, the AE signals have been classified into two categories. The two signatures were named T1 signature and T2 signature. Examples of T1 and T2 signatures (recorded at PWAS 1) are presented in Figure 8. The signature T1 was observed to have a broadband frequency spectrum as we observe in Figure 8, whereas the signature T2 was observed to have a valley between 200 to 400 kHz and two peaks before and after the valley (50-150 kHz and 400-500 kHz). The strength of the peak between 400-500 kHz was observed to have variations for different signals. T1 signature was very frequently appearing when active crack growth was happening during the fatigue experiment and T2 signature when no crack growth occurred. So the T1 signature was hypothesized to be due to fatigue crack growth event and T2 signature due to fatigue crack rubbing/clapping.

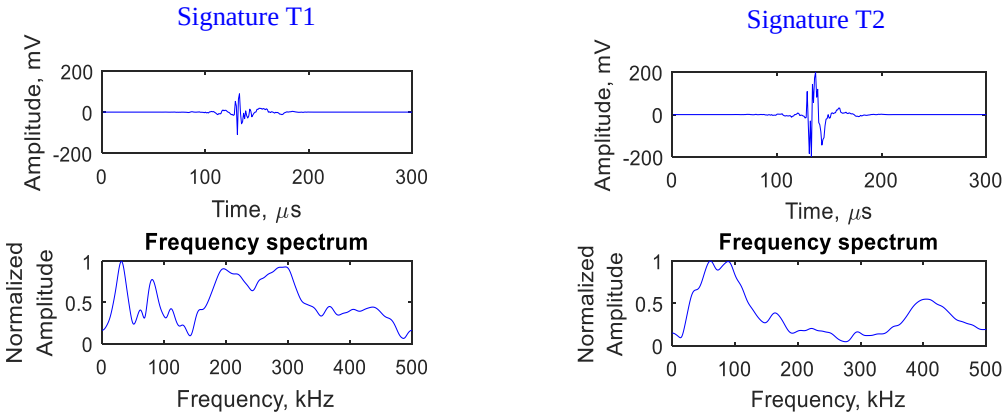

Figure 8 Two major class of AE signal signatures observed during the experiment

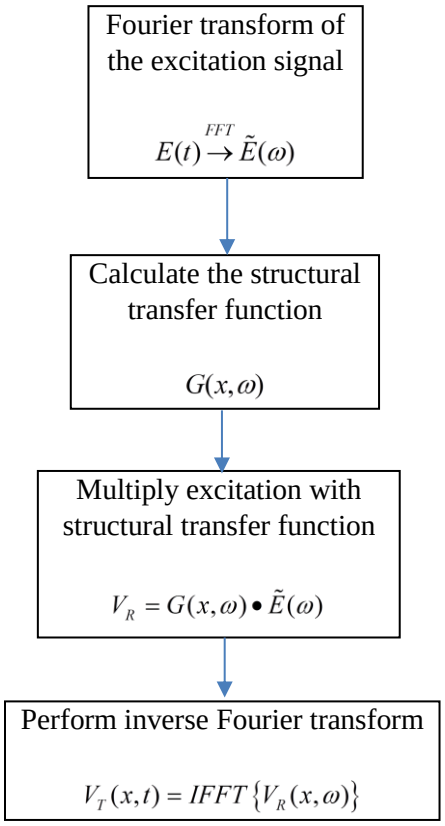

Figure 9 Predictive simulation of AE signal: flow chart

Assuming an erf-function-excitation [20], numerical simulation of the AE signal at the receiver PWAS was performed by using the steps in the predictive simulation flow chart in Figure 9. For an M_{12} excitation, the structural transfer function was derived in Eq. (6). The structural transfer function used was as following.

$$G(x,\omega) =\cdot \frac{g_{31}^2}{(s_{11}^E \beta_{33}^T C_c)} \sum_m \frac{F_x}{4P_{mm}} \left[v_m(y)(\tilde{v}_x^m(y)_{-d}^{+d}) + \frac{\partial}{\partial y} v_m(y) \int_{-d}^{d} \tilde{v}_x^m(y) dy \right] \times (e^{-i\xi_m(r_c+2s_r)} - e^{-i\xi_m(r_c)})/i\omega \quad (7)$$

Adjusting the erf-function rise-time, the crack rubbing/capping AE signal examples received during the cyclic fatigue loading were reproduced. Figure 10 presents the adjusted erf function excitation, experimental AE signal example (recorded at PWAS 2) and the numerical simulation. A rise time of 2.5 μs was used to obtain the AE signal simulation similar to the experimental AE signal. As we observe, a very good match of the experimental observation and simulation was achieved. As the theoretical simulation predicted, the experimental fatigue-crack rubbing/clapping signal also has a strong A0 mode content.

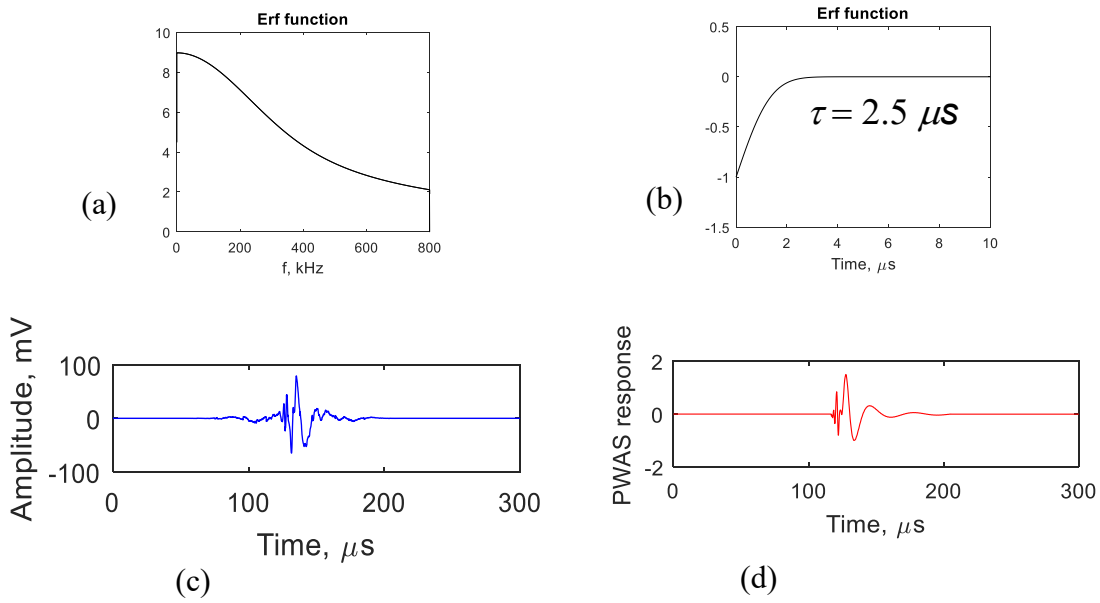

Figure 10 Fatigue crack rubbing/clapping AE simulation example a) Time-domain erf function excitation b) Frequency domain of erf function c) Experimental observation d) Theoretical prediction

6 SUMMARY CONCLUSIONS AND FUTURE WORK

6.1 SUMMARY

Fatigue crack experiment was performed to record AE signals during the fatigue crack growth. Analysis of the AE signals was performed to classify the signals. AE signal simulation for a fatigue crack rubbing/clapping event was performed. M_{12} moment excitation was considered for the simulation of fatigue crack-rubbing/clapping.

6.2 CONCLUSIONS

Two broad classes of AE signal signatures were identified based on the analysis. The signal signature classes were named as T1 and T2. T1 had a broadband characteristic in the frequency domain, whereas T2 had a valley between 200 to 400 kHz and two peaks before and after the valley (50-150 kHz and 400-500 kHz). The T1 signature was frequently appearing during the

active crack growth situation. No T1 was observed when crack was not growing. Because of these reasons, the T1 signature is thought to be the fatigue crack growth AE signature. The T2 signature was recorded even when the crack was not growing. Because of this reason, the T2 signature is thought to be the signature due to crack rubbing/clapping. Analytical prediction of fatigue crack rubbing/clapping AE signals using the M_{12} moment excitation concept was performed. M_{12} moment tensor components excite strong A0 mode, and no S0 mode was produced theoretically. A good match of the experimental observation and numerical prediction was observed.

6.3 FUTURE WORK

In the future, FEM analysis of fatigue crack growth and fatigue crack rubbing/clapping will be performed using the moment tensor concept.

7 ACKNOWLEDGMENTS

This work was supported by the Office of Naval Research (ONR) grant number N00014-17-1-2829.

8 REFERENCES

[1] M. Y. Bhuiyan and V. Giurgiutiu, "The signatures of acoustic emission waveforms from fatigue crack advancing in thin metallic plates," *Smart Mater. Struct.*, vol. 27, no. 1, p. 15019, 2018.

[2] H. Mei, M. Haider, R. Joseph, A. Migot, and V. Giurgiutiu, "Recent Advances in Piezoelectric Wafer Active Sensors for Structural Health Monitoring Applications," *Sensors*, vol. 19, no. 2, p. 383, 2019.

[3] Q. Wang and F. Chu, "Experimental determination of the rubbing location by means of acoustic emission and wavelet transform," *J. Sound Vib.*, vol. 248, no. 1, pp. 91–103, Nov. 2001.

[4] M. Bentahar and R. El Guerjouma, "Monitoring progressive damage in polymer-based composite using nonlinear dynamics and acoustic emission," *J. Acoust. Soc. Am.*, vol. 125, no. 1, pp. EL39-EL44, 2009.

[5] M. G. R. Sause, A. Gribov, A. R. Unwin, and S. Horn, "Pattern recognition approach to identify natural clusters of acoustic emission signals," *Pattern Recognit. Lett.*, vol. 33, no. 1, pp. 17–23, Jan. 2012.

[6] S. M. Cousland and C. M. Scala, "Acoustic emission during the plastic deformation of aluminium alloys 2024 and 2124," *Mater. Sci. Eng.*, vol. 57, no. 1, pp. 23–29, Jan. 1983.

[7] J. J. Ditri and J. L. Rose, "Excitation of guided elastic wave modes in hollow cylinders by applied surface tractions," *J. Appl. Phys.*, vol. 72, no. 7, pp. 2589–2597, 1992.

[8] R. Joseph, M. Y. Bhuiyan, and V. Giurgiutiu, "Acoustic emission from vibration of cracked sheet-metal samples," *Eng. Fract. Mech.*, vol. 217, no. July, p. 106544, 2019.

[9] S. L. McBride, J. W. MacLachlan, and B. P. Paradis, "Acoustic emission and inclusion fracture in 7075 aluminum alloys," *J. Nondestruct. Eval.*, vol. 2, no. 1, pp. 35–41, 1981.

[10] C. Barile, C. Casavola, and G. Pappalettera, "Acoustic emission waveform analysis in CFRP under Mode I test," *Eng. Fract. Mech.*, no. December 2017, pp. 0–1, 2018.

[11] S. B. M. Saadatzi, F. Mir, M. N. Saadatzi, V. Tavaf, "Modeling of a 3D acoustoelastic metamaterial energy harvester," in *Active and Passive Smart Structures and Integrated Systems XII*, 2018.

[12] S. B. M. Saadatzi, F. Mir, M. N. Saadatzi, "Modeling and Fabrication of a Multi-axial Piezoelectric Energy Harvester based on a Metamaterial-inspired Structure," *IEEE Sens. J.*, vol. 18, no. 22, 2018.

[13] S. B. M. Saadatzi, M. N. Saadatzi, R. Ahmed, "An electro-dynamic 3-dimensional vibration test bed for engineering testing," in *Industrial and Commercial Applications of Smart Structures Technologies*, 2017.

[14] R. Joseph, M. Y. Bhuiyan, and V. Giurgiutiu, "Acoustic emission source modeling in a plate using buried moment tensors," *Proc. SPIE (Health Monit. Struct. Biol. Syst.*, vol. 10170, no. May, pp. 1017028-1–8, 2017.

[15] R. Joseph *et al.*, "Active health monitoring of TN32 dry cask using a scaled down model," *Proc. SPIE (Health Monit. Struct. Biol. Syst*, no. March, 2018.

[16] M. G. R. Sause and S. Horn, "Simulation of Acoustic Emission in Planar Carbon Fiber Reinforced Plastic Specimens," *J. Nondestruct. Eval.*, vol. 29, no. 2, pp. 123–142, 2010.

[17] M. Åberg, "Numerical modeling of acoustic emission in laminated tensile test specimens," *Int. J. Solids Struct.*, vol. 38, pp. 6643–6663, 2001.

[18] G. J. Prosser WH, Hamstad MA, "Finite Element and Plate Theory Modeling of Acoustic Emission Waveforms," *J Nondestruct Eval*, vol. 18, pp. 83–90, 1999.

[19] A. Zelenyak, M. Hamstad, and M. Sause, "Modeling of Acoustic Emission Signal Propagation in Waveguides," *Sensors*, vol. 15, no. 5, pp. 11805–11822, 2015.

[20] M. A. Hamstad, A. O'Gallagher, and J. Gary, "Modeling of buried monopole and dipole sources of acoustic emission with a finite element technique," *J. Acoust. Emiss.*, vol. 17, no. 3/4, pp. 97–110, 1999.

[21] J. R. Rice, "Elastic wave emission from damage process," *J. Nondestruct. Eval.*, vol. 1, no. 4, pp. 215–224, 1980.

[22] A. Keiiti and G. Paul, *Quantitative Seismology*. University Science Books, 2002.

[23] Y. Haider, M. F., Giurgiutiu, V., Lin, B. and Yu, "Simulation of Lamb Wave Propagation using Excitation Potentials," in *ASME 2017 Pressure Vessels & Piping Conference*, 2017.

[24] R. Joseph, "Acoustic emission and guided wave modeling and experiments for structural health monitoring and non-destructive evaluation," Univeristy of South Carolina, 2020.